ACS APPLIED MATERIALS & INTERFACES

Research Article

www.acsami.org

Oligolayer-Coated Nanoparticles: Impact of Surface Topography at the Nanobio Interface

Eva-Christina Wurster,[†] Renate Liebl,[†] Stefanie Michaelis,[‡] Rudolf Robelek,[‡,§] Daniel S. Wastl,[∥] Franz J. Giessibl,[∥] Achim Goepferich,[†] and Miriam Breunig*[,†]

[†]Department for Pharmaceutical Technology, [‡]Department for Analytical Chemistry and Biosensors, and [∥]Institute of Experimental and Applied Physics, University of Regensburg, Universitätsstrasse 31, 93053 Regensburg, Germany

Supporting Information

ABSTRACT: Layer-by-layer coating of nanoparticles with a layer number in the single-digit range has gained increasing attention in the field of nanomedicinal research. However, the impact of using various polyelectrolytes on oligolayer formation and, more importantly, their influence on the interaction with the biological system has not often been considered in the past. Hence, we investigated the polyelectrolyte deposition profiles and resulting surface topographies of up to three polyelectrolyte layers on a flat gold sensor surface using three different polycations, namely, poly(ethylene imine) (PEI), poly(allylamine hydrochloride) (PAH), and poly(diallylammonium chloride) (PD), each in combination with poly(styrenesulfonate) (PSS). Surface plasmon resonance spectroscopy and atomic force microscopy revealed that the PEI/PSS pair in particular showed a so-called overshoot phenomenon, which is associated with partial polyelectrolyte desorption from the surface. This is also reflected by a significant increase in the surface roughness. Then, after having transferred the oligolayer assembly onto nanoparticles of ~32 nm, we realized that quite similar surface topographies must have emerged on a curved gold surface. A major finding was that the extent of surface roughness contributes significantly to the fashion by which the oligolayer-coated nanoparticles interact with serum proteins and associate with cells. For example, for the PEI/PSS system, both the surface roughness and protein adsorption increased by a factor of ~12 from the second to third coating layer and, at the same time, the cell association massively decreased to only one-third. Our study shows that surface roughness, along with other particle properties such as size, shape, zeta potential, and hydrophobicity, is another decisive factor for nanoparticles in a biological context, which has indeed been discussed previously but has not to date been investigated for oligolayers.

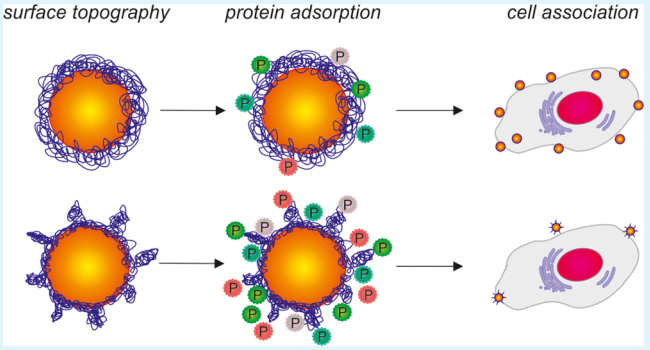

KEYWORDS: *Layer-by-layer, planar surface, AFM, nanoparticle, protein adsorption, cell association*

INTRODUCTION

Layer-by-layer (LbL) assembly is a powerful tool for the functional modification of surfaces and has gained significant interest for various biomedical applications.[1−3] It is based on the alternating deposition of oppositely charged polyelectrolytes or other multivalent species on solid surfaces. Initially, the LbL technique focused solely on the formation of films on macroscopic flat surfaces and involved an extensive series of deposition cycles leading to polyelectrolyte multilayers with up to 30 bilayers or more.[4,5] Because polyelectrolyte deposition on flat surfaces is highly efficient and rapid, the formation of very complex and rather thick multilayers with completely new structural and dynamic features was easily accomplished.[4,5]

In contrast, on curved surfaces in the sub-100 nm range, the generation of multilayer films was recognized as a tremendous challenge due to several time-consuming washing steps and the probability of producing particle aggregates.[6,7] Therefore, it is not surprising that reducing the layer number to the lower single-digit range became a priority as soon as LbL-coated nanoparticles were identified as a favorable tool for the delivery of macromolecular drugs, such as nucleic acids.[8−12] As an example, we were the first to report a delivery system for nucleic acids with only two or three polyelectrolyte layers assembled on gold nanoparticles.[8,13] Similarly, Tan et al. developed hydroxyapatite nanoparticles coated with poly(L-arginine), dextran, and small interfering RNA.[12] In addition to facilitating particle up-scaling, which would be a requirement for possible clinical applications,[14] this limitation to size of fabricated oligolayers is important for another reason: endocytosis by living cells requires a narrow particle size window with an optimum size of less than ~80 nm.[13,15] Because each bilayer adds a substantial size increment to the hydrodynamic diameter of the nanoparticles, especially if a

Received: December 1, 2014
Accepted: March 27, 2015
Published: March 27, 2015

DOI: 10.1021/am508435j
ACS Appl. Mater. Interfaces 2015, 7, 7891−7900

nucleic acid with a large persistence length is applied,[8] a coating process with as few layers as possible is envisioned.

Despite the growing number of publications in the field of oligolayer-coated nanoparticles for drug delivery, the influence of different polyelectrolytes on the formation of the oligolayers and, more importantly, their impact on interactions with biological systems has not to date been evaluated in a comparative study. Therefore, we investigated the oligolayer deposition profiles of three different polycation-coating series in detail. For this purpose, we compared the oligolayer formation on a flat surface because it is more accessible to generally applied LbL characterization methods, such as surface plasmon resonance (SPR) spectroscopy and atomic force microscopy (AFM). Then, we transferred the oligolayer assembly on nanoparticles of ∼32 nm. Here, we focused on the resulting surface topography with respect to protein adsorption and cell association. Surface roughness is a decisive factor for nanoparticles in a biological context that to date has indeed been discussed[16,17] but not investigated for oligolayers in detail. Obtaining more detailed insight on the formation and interaction of such oligolayers with biological systems will help to evaluate the potential of future LbL-based therapeutic nanomedicinal delivery applications.

EXPERIMENTAL SECTION

Materials. If not otherwise stated, all chemicals were purchased from Sigma-Aldrich Chemical Co. (Taufkirchen, Germany). The polyelectrolytes had the following molecular weights: poly(allylamine hydrochloride), 17000 g/mol; branched poly(ethylenimine), 25000 g/mol; poly(diallyldimethylammonium chloride), <100000 g/mol; poly(styrenesulfonate sodium salt), 15000 g/mol (Polymer Standard Service, Mainz, Germany). Ultrapure water was obtained using a Milli-Q-System (Merck Chemicals, Schwalbach, Germany).

Surface Plasmon Resonance (SPR) Spectroscopy. High refractive index glass slides covered with a 5 nm chromium bottom and a 45 nm thick top gold layer were used as substrates for surface plasmon excitation. Sensor slides were rinsed with 70% ethanol, air-dried, and plasma treated for 2 min inside an Ar plasma generator (Harrick Plasma, NY; USA). The cleaned and activated sensor slides were then immersed in 1 mg/mL 11-mercatoundecanoic acid (MUA) for 3 days and then dried in a nitrogen stream. The SPR measurements were performed with a Biosuplar 400T SPR system (MiviTec GmbH, Sinzing, Germany) at 37 °C. To this end, the SPR substrates were mounted to the prism coupler of the system using immersion oil (n = 1.61; Cargille Laboratories, Cedar Grove, NJ, USA). A homemade flow cell consisting of a 1 mm PDMS spacer and an appropriate flow cell cover with inset in- and outlets coupled to a syringe pump (TSE Systems, Bad Homburg, Germany) was used. A constant flow rate of 100 μL/min was applied. The completed sensor architecture was equilibrated with ultrapure water. After obtaining stable baseline signals, the MUA layer on the sensor surface was activated by 0.01 M NaOH followed by a rinsing step. Four hundred microliters of each polyelectrolyte was successively added to the system, which was always followed by a water rinsing step until a stable SPR signal was achieved. Polymer concentrations were 1 mg/mL.

The SPR system was run in the angle or kinetic measurement mode. For the angle measurement mode, a full angular scan (θ = 58−68°) was performed after each polyelectrolyte incubation step. In the kinetic measurement mode, changes in reflectivity (Δ reflectivity) were recorded over time at a constant SPR observation angle. The observation angle used was extracted from the first complete angle scan curve recorded from the SPR sensor after its activation. In both measurement modes, data was recorded using the manufacturer's software and exported to the software Origin6 (OriginLab, Northampton MA, USA) for further analysis. Data evaluation of the SPR angle scan curves for the calculation of the layer thicknesses was performed by a Maxwell equation mechanism using the free software tool "Winspall". Further theoretical details and the optical parameters used can be found in the Supporting Information.

Quartz Cantilever Atomic Force Microscopy (AFM). The AFM experiments were performed on a home-built qPlus ambient FM-AFM system operated by a Nanonis Control System with an OC4 phase-locked loop (SPECS GmbH, Berlin, Germany).[18−21] Custom designed qPlus sensors were used that were manufactured similarly to quartz tuning forks.[22,23] The sensors had a characteristic resonance frequency of f_0 = 32768 Hz and a stiffness k = 1280 N/m. The qPlus Sensors were equipped with silicon tips made by splintering bulk crystals. Sensor parameters were f_0 = 29734 Hz and Q_{air} = 2364 with a bulk silicon tip. This tip is extremely thin and lasts for only a limited number of measurements. Because every change of the tip affects the comparability, all images were measured with the same tip instead of measuring more than one sample per preparation condition. However, to ensure that outliers were not measured, the layer build-up of the AFM samples was performed in the SPR measuring cell. Hence, the SPR graphs were an optimal quality criterion for the layer assembly. The surface roughness was quantified by extracting the roughness root-mean-square (Rq) with WSxM v4.0 Beta 7.0 software (Nanotec Electronica S.L., Tres Cantos, Spain).[24]

Particle Synthesis, LbL Modification, and Characterization. The particle synthesis and coating protocol has already been published in detail.[25] In brief, 30 nm gold nanoparticles (AuNP) were synthesized by citrate reduction as follows: 2 mL of 1% (w/v) aqueous sodium citrate trihydrate (Merck KGaA, Darmstadt, Germany) solution was added to a boiling solution of 0.1% (w/v) gold(III) chloride under vigorous stirring. The conditions were kept constant for 10 min until the red color of colloidal gold appeared. The citrate ligands were subsequently exchanged with MUA by adjusting the pH to 11 with 1 M NaOH and the addition of 0.1 mg/mL MUA in ethanol. The particle suspension was stirred at ambient temperature for 3 days to achieve a stable thiol bond to the gold surface. For the LbL modification, particles were purified by several centrifugation steps. The purification protocol was adjusted from Balasubramanian.[26] The suspensions were centrifuged at 6000 g for 10 min at 4 °C, and the pellets were resuspended in water. The centrifugation speed was reduced by 500 g with each polymer layer. The LbL coating procedure was as follows: Purified AuNPs were added dropwise to a stirring solution of the polyelectrolyte to give a final concentration of 1 mg/mL of the polyelectrolyte, which was stirred for an additional 30 min. Then, the particles were purified by centrifugation as described above and immediately coated with the next polyelectrolyte. The nanoparticles were characterized by their hydrodynamic diameter and zeta potentials using a Zetasizer Nano ZS (Malvern Instruments, Herrenberg, Germany). For size measurements, 173° backward scattering in general purpose mode was applied, and the maximum peak of the intensity distribution is always stated. The zeta potential measurements were processed in the monomodal mode. For light scattering and zeta potential measurements, the pH was neutral, and the ionic strength was comparably low because no ions were added to the samples. Visible spectrometry (UVIKON 941, Kontron, now Goebel Instrumentelle Analytik, Au/Hallertau, Germany) was used to determine the surface plasmon peak of the colloidal gold to calculate the AuNP particle concentration.[27]

Gel Electrophoresis. Equal amounts of purified LbL-coated gold nanoparticles were incubated with Leibovitz Medium containing 10% FCS at 37 °C for 1 h. The particles and unadsorbed serum proteins were separated by centrifugation (5 °C, 15000 g, 60 min). Thereafter, the pellet was washed three times in ice-cold Millipore water (5 °C, 9500 g, 30 min). The purified samples were analyzed by sodium dodecyl sulfate polyacrylamide gel electrophoresis (SDS-PAGE) on a 15% poly(acrylamide gel). SDS in the sample buffer removed the protein corona from the particles.[28] The electrophoresis was run at 120 V for 45 min using a Pharmacia EPS 600 gel electrophoresis device (Bio-Rad Laboratories, Munich, Germany) and subsequently stained with Coomassie Blue. The protein molecular weight standard was an unstained protein marker with a molecular weight range from 14.4 to 116.0 kDa (#26610, Thermo Fisher Scientific, Schwerte, Germany). The gels were imaged using a BioRad Imaging System

DOI: 10.1021/am508435j
ACS Appl. Mater. Interfaces 2015, 7, 7891−7900

(ChemiDoc XRS+, BioRad, München, Germany) and evaluated with Lab Image Software (BioRad, München, Germany). The band intensities were calculated using the BSA band (66.2 kDa) and the molecular weight marker as references. Protein bands were detected by the default band detection tool with high resolution settings.

Cell Culture and Cellular Association. HeLa cells (ATCC: CCL-2) were cultured in 75 cm^2 culture flasks at 37 °C in a 5% CO_2 humidified environment in Eagle's Minimum Essential Medium with 10% serum pyruvate (110 mg/L) (EMEM+). Cellular association of nanoparticles was measured by a photometric assay based on the absorption of gold nanoparticles in Leibovitz medium (Invitrogen, Life Technologies, Darmstadt, Germany, with 10% serum and without phenol red). The method was first published by Cho et al. and calculates the amount of cell-associated particles by the reduced absorption of gold nanoparticles after incubation with cells[29,30] as follows.

In brief, the absorption (Abs) of the cell culture medium containing AuNP before (0) and after (t) the incubation time for a cell containing the sample and a control without cells was measured at 506 nm. Thereafter, we calculated the loss of nanoparticles due to unspecific adsorption ($Loss_{control}$) and to cell association ($Loss_{w/cells}$) using eq 1.

$$\text{Loss\%} = 100 - \left(\frac{Abs_t}{Abs_0} \times 100\right) \quad (1)$$

The difference of the two samples gave the percentage of cell-associated particles as shown in eq 2.

$$\text{Cell Association (\%)} = \text{Loss\%}_{w/cells} - \text{Loss\%}_{control} \quad (2)$$

Using this percentage together with the added molar concentration of gold nanoparticles (c_0) and the Avogadro constant (N_A), the absolute number of associated particles (N_{assoc}) per liter was calculated (eq 3).

$$N_{assoc} = (c_0 \times \text{Cell Association\%}) \times N_A \quad (3)$$

Subsequently, the number of associated particles in the incubation volume was calculated. In addition, the cell number was determined by counting in a Neubauer Chamber. Finally, the number of associated particles in the incubation volume was divided by the number of cells, which resulted in the number of associated particles per cell (AuNP/cell).

In our case, an internal standard of 20 pM coated AuNP was added to all photometric samples to increase the absorption values over the detection limit. This internal standard was incubated with cell culture medium containing 10% serum 1 h prior to the absorption measurement to ensure the formation of a protein corona around the particles and comparable absorption spectra. As a control for unspecific adsorption of gold nanoparticles to the cell culture material, the incubation was performed without cells and subtracted from the cell-containing samples. For practical reasons, cell association studies of concentrations of 2.5 pM and higher could only be performed in duplicates. The photometric samples were analyzed using a double-beam photometer at 506 nm (UVIKON 941).

Statistics. All experiments were performed with two to four replicates, and the results are given with standard deviation. For SPR, AFM, and SDS-PAGE, a representative example is shown. One-way ANOVA followed by a Student–Newman–Keuls (SNK) test was performed using SigmaPlot 12.0 (Systat Software Inc, San José, CA, USA) to test statistical significance.

RESULTS AND DISCUSSION

In this study, the deposition of three different polycations in combination with poly(styrenesulfonate) (PSS) as a polyanion on a gold surface (either flat or curved) was investigated. In the first step, the gold surface was functionalized using 11-mercaptoundecanoic acid (MUA) to yield a permanent negative surface charge for further deposition of the oppositely charged polyelectrolytes. Then, formation of the oligolayer started with a polycation, followed by the polyanion PSS, and a terminal polycation layer. Poly(ethylene imine) (PEI), poly(allylamine hydrochloride) (PAH), and poly(diallylammonium chloride) (PD) were chosen as polycations to give three different final coating series. These polycations primarily differ in their architecture, functional amino groups, pK_a values, and molecular weights (MWs) (Table 1).

Table 1. Overview of the Polyelectrolytes Used for the Formation of Oligolayers on a Gold Surface

	PEI	PAH	PD	PSS
structure	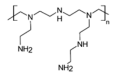			
architecture	branched	linear	linear	linear
amines	1°, 2°, 3°	1°	4°	-
pKa	8.5[30]	9.7[31]	-	1[32]
MW (kDa)	25	15	<100	15

PEI is a highly charged branched polymer carrying primary, secondary, and tertiary amines and is known to be a suitable transfection agent for nucleic acids.[14,34] PAH is a linear polyelectrolyte with only primary amino groups. In contrast, PD consists of quaternary amines and is therefore completely charged independent of the pH of the surrounding medium. The polyanion PSS with a molecular weight of 15 kDa was chosen as a surrogate for any negatively charged macromolecules and can easily be replaced by therapeutic nucleic acids to design a drug delivery system.[8,13,15]

The oligolayer formation on a flat gold surface was monitored by SPR spectroscopy. To this end, the kinetic profiles were recorded by measuring the change in reflectivity (Δ reflectivity) over time (Figure 1 A–C). In the case of the PAH- and PD-series, each polymer deposition yielded a plateau in the Δ reflectivity curves (Figure 1 B,C). Finally, after the oligolayer was completed, a "stair-like" deposition profile was observed. The corresponding layer thicknesses, which were calculated by a Maxwell equation fit, increased with each polymer layer, and the final thickness after three polymer layers was ∼4.7 nm for the PAH-series and ∼3.6 nm for the PD-series (Figure 1 E,F). Altogether, these SPR profiles fit to regular polyelectrolyte multilayer assemblies where an increase in the thickness of each layer is characteristic.[35−38] In addition, the calculated layer thickness of the PAH-series is in very good agreement with the literature[39,40] and thus corroborates the applicability of SPR measurements. In contrast, the PEI-series only followed this regular deposition until the second layer. Upon deposition of the third layer, a sharp peak appeared, which was followed by a rapid decrease in Δ reflectivity (Figure 1 A). This was also reflected by the thickness, which was ∼10 nm after two layers but collapsed to ∼1.6 nm for the trilayered PEI/PSS/PEI system (Figure 1 D). For data fitting to obtain the layer thickness, it was assumed that the layers do not merge. It should be noted that the value of the trilayered PEI/PSS/PEI-system is consequently afflicted with some uncertainty. Such a characteristic deposition curve, which deviates from the stair-like shape, was already published by the group of Cohen Stuart for a salt-dependent LbL system of poly(acrylic acid) and poly(dimethylaminoethyl methacrylate)[41] and was theoretically investigated even earlier by the Filippova group.[42] In more detail, Cohen Stuart described a stepwise process, which involved the deposition of the polycation, followed by its

DOI: 10.1021/am508435j
ACS Appl. Mater. Interfaces 2015, 7, 7891−7900

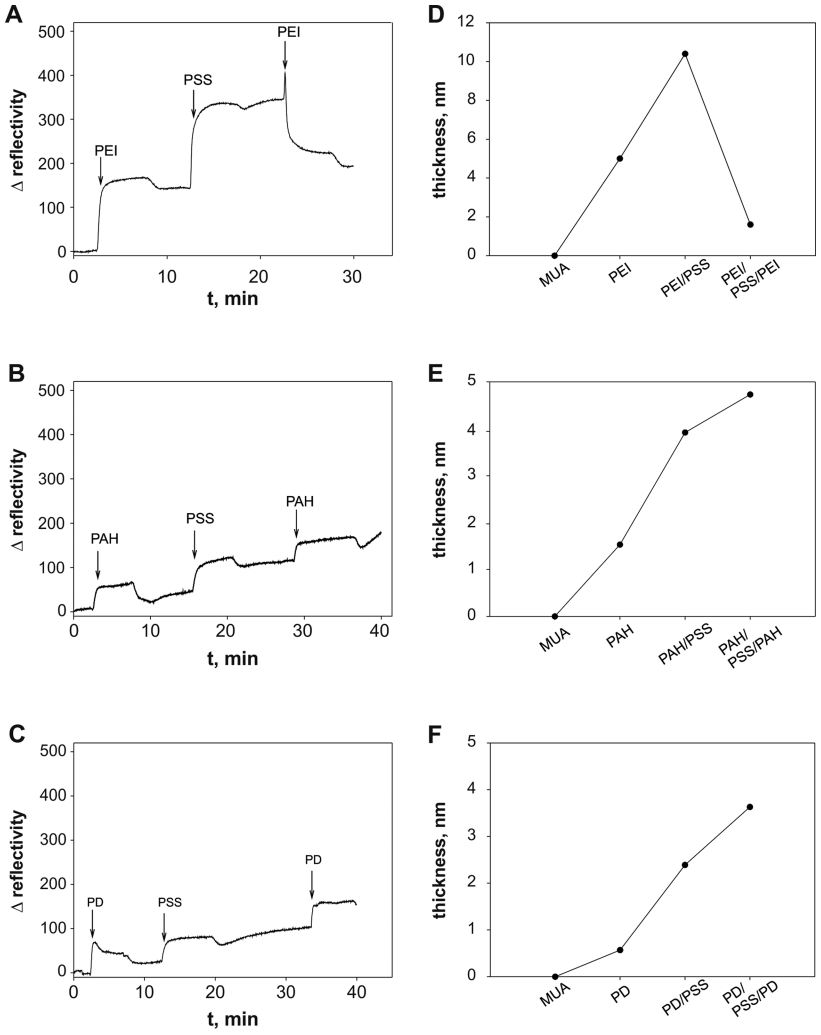

Figure 1. Deposition profiles of the different polyelectrolyte pairs measured by SPR spectroscopy on a gold sensor surface. An arrow indicates the addition of each polymer to the flow cell. The moderate decrease of Δ reflectivity after each polymer deposition is due to a water rinsing step. (A) In the PEI-series, the first and second layer adsorbed stepwise but the third layer was not successfully adsorbed. A decrease in Δ reflectivity and collapse of the oligolayer occurred. (B and C) The PAH- and PD-series showed a characteristic stair-like increase of Δ reflectivity as well as an increase in layer thickness with each polymer layer. (D–F) The corresponding calculated layer thicknesses for the three coating series. Note the variable scaling of the *y*-axis.

mixing with the layer beneath, then a formation of polyelectrolyte complexes and finally a polyelectrolyte erosion from the surface.[41]

These so-called overshoots are still under scientific discussion,[43,44] and it has not been clarified if only a layer collapse or if layer detachment is also involved. To the best of our knowledge, the effect was only discussed for the polyelectrolyte pair mentioned above. Here, we show that the presented PEI/PSS pair might be another example of this phenomenon, particularly because it was not possible to avoid the decrease in Δ reflectivity by varying the PEI concentration used (data not shown). The type of polyanion used seemed to play an important role because exchanging the strong polyelectrolyte PSS (pK_a 1)[33] with the weak polyelectrolyte poly(acrylic acid) (PAA) (pK_a 4.5)[45] did not result in this overshoot phenomenon (Supporting Information, Figure S1).

We speculate that overshoot of the PEI-series would most likely result in a very heterogeneous surface structure. To this end, cantilever AFM[19] was used to visualize the surface of the previously coated SPR substrates and to evaluate the effect of the irregular polyelectrolyte deposition in the PEI-series. The MUA functionalized gold substrate was observed as the control (Figure 2 A). This surface showed diagonal rills and irregular heights and consequently proved to be a valuable indicator of successful surface coverage for subsequent polyelectrolyte deposition. Similarly to the SPR measurements, the AFM images revealed differences between the PEI-series and the PAH- and PD-series, and differences in the polymer characteristics were retrieved. The PAH- and PD-series indicated a regular layer build-up with increasing polymer adsorption with an increasing number of layers. Because the characteristic diagonal rills of the gold substrate were still visible through polymer coating of the bilayered PAH/PSS, it was concluded that these two polymer layers were not sufficient to completely cover the gold substrate (Figure 2 C). Moreover, at this coating stage, the sample was sprinkled with structures that were attributed to polymer aggregates. However, these structures were leveled out upon the addition of the third polymer layer; the rills were no longer visible and the PAH/PSS/PAH surface was quite smooth (Figure 2 F). Thus, in the PAH-series, at least three polymer layers were necessary for complete coverage of the gold substrate. In the PD-series, the diagonal rills of the

DOI: 10.1021/am508435j
ACS Appl. Mater. Interfaces 2015, 7, 7891–7900

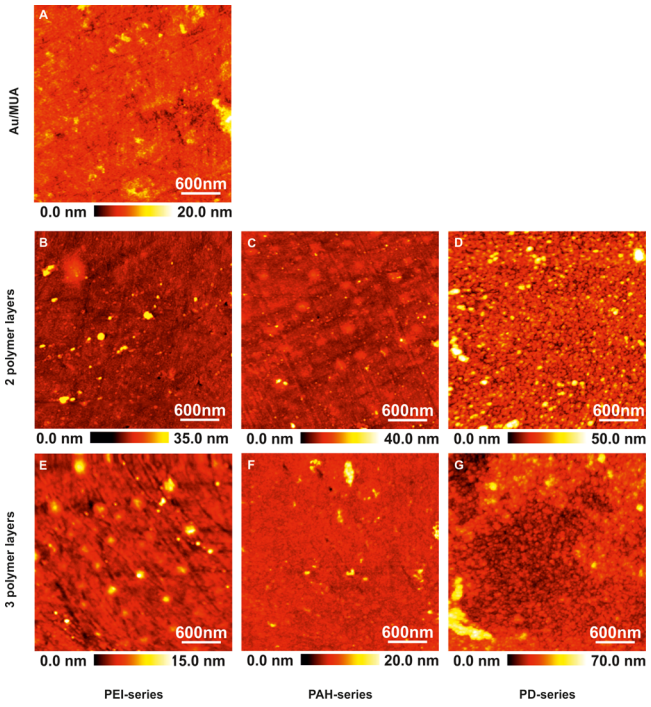

Figure 2. AFM images of coated gold surfaces: (A) Control gold surface modified with MUA, (B) PEI/PSS, (C) PAH/PSS, (D) PD/PSS, (E) PEI/PSS/PEI, (F) PAH/PSS/PAH, and (G) PD/PSS/PSS. PD-surfaces (D, G) completely covered the gold substrate, whereas the bilayered PAH/PSS (C) and the trilayered PEI/PSS/PEI (E) surface only partially covered the template. Additional high-resolution AFM images can be found in the Supporting Information, Figures S2 and S3. In addition, to demonstrate reproducibility, more images of the PEI-series can be found in the Supporting Information, Figure S4. Scan parameters: frequency shift Δf = +10 to +12 Hz; oscillation amplitude A = 300 pm.

gold substrate were completely covered at each coating step. The images are characterized by the occurrence of regular protrusions. Because the AFM technique has the potential for resolution down to the atomic scale, we attributed these protrusions to loops and coils of the PD polymer chain (for high resolution images of the regular protrusions, see the Supporting Information, Figures S2 and S3). These characteristic nanostructures have already been reported for higher layer numbers on silica substrates.[46] The high molecular weight and the fact that PD is completely charged leads to strong electrostatic repulsion of the polymer segments, leading to a coiled surface conformation (Figure 2 D, G).[47,48] As the bilayered sample already showed this characteristic nanostructure, it can be assumed that even a single layer of PD is most likely sufficient to completely cover the surface features of the gold substrate. The most interesting behavior was found for the samples of the PEI-series. The bilayered PEI/PSS surface was quite smooth aside from a few aggregates, and furthermore, the structures of the gold substrate were to a large degree covered. However, the trilayered PEI/PSS/PEI surface again showed the characteristic rill structure of the substrate in the presence of sharp surface features ~15 nm in height (Figure 2 E). Comparing the PEI/PSS/PEI sample with the bilayered PEI/PSS surface (Figure 2 B), it is obvious that these characteristic structures must appear upon the addition of the third layer by partial desorption of the previously adsorbed polymer. It should be noted that the SPR measurements and AFM images cannot be compared on the same height scale because SPR averages data over an area of 1 mm^2 whereas AFM measurements are space-resolved, thereby identifying single interesting surface structures. Nevertheless, the AFM images were in good agreement with the SPR measurements and supported the hypothesis of a possible overshoot phenomenon with the formation of polyelectrolyte complexes and partial desorption of the polyelectrolytes.

To substantiate these distinct differences in the surface topology within one coating series as well as between the polycations, we determined the root-mean-square roughness (Rq) of each sample (Table 2). The surface roughness of the

Table 2. Root-Mean-Square Roughness (Rq) Extracted from the AFM Images[a]

	PEI-series (nm)	PAH-series (nm)	PD-series (nm)
second layer	8.08	17.31	21.58
third layer	94.84	14.76	29.12

[a]Because the Rq values were averaged over a region of 1 × 1 μm of one representative sample, no error estimation is available.

PD-series only slightly increased during the coating procedure. Because the surface topography was regular on each layer, the Rq did not show any large differences. The bilayered PAH/PSS surface exhibited some yellow spots on its surface, indicating specific surface heights, whereas the trilayered PAH/PSS/PAH surface showed homogeneous red coloring, which was supported by a marginal decrease of Rq from approximately 17 to 15 nm. In contrast, this trend was reversed in the PEI-series, where Rq increased from ~8 nm in the bilayered case to ~95 nm in the trilayered, roughest surface. To our knowledge, this is the first report of these structural surface features for three polycations being compared at such a low number of layers.

To evaluate if these interesting surface topographies had an impact on functionality in a biological context, we substituted the macroscopic planar gold surface by gold nanoparticles with high surface curvature. This step is necessary to achieve a size order suitable for cell association. To this end, gold nanoparticles of ~32 nm were chosen as substrates because this size is close to optimum for cellular uptake of nanoparticles.[13,15] To monitor the success of coating the nanoparticles with oppositely charged polyelectrolytes, we made use of two standard techniques for nanoparticle characterization, which are hydrodynamic diameter and zeta potential (Figure 3). During the coating process with MUA and the polyelectrolytes, the sign of the zeta potential was converted with each polymer layer, indicating successful deposition of oppositely charged polyelectrolytes (Figure 3 A). The hydrodynamic diameter increased stepwise with each layer for the PAH- and PD-series comparable to the SPR measurements (Figure 3 B). This size increase of 11 nm or less per layer was due to polymer adsorption and not to particle aggregation because aggregation would have led to larger particle multiplicates and therefore to a much greater shift in the particle size distribution.[6,7] A peculiarity was found for particles of the PEI-series; a size decrease of ~5 nm instead of further particle growth was observed upon the addition of the third polymer layer. Of course the layer thicknesses that were calculated from the SPR measurements on a flat surface can only be qualitatively compared to the hydrodynamic diameter of a colloid, but we postulate that both the size decrease of PEI-

DOI: 10.1021/am508435j
ACS Appl. Mater. Interfaces 2015, 7, 7891−7900

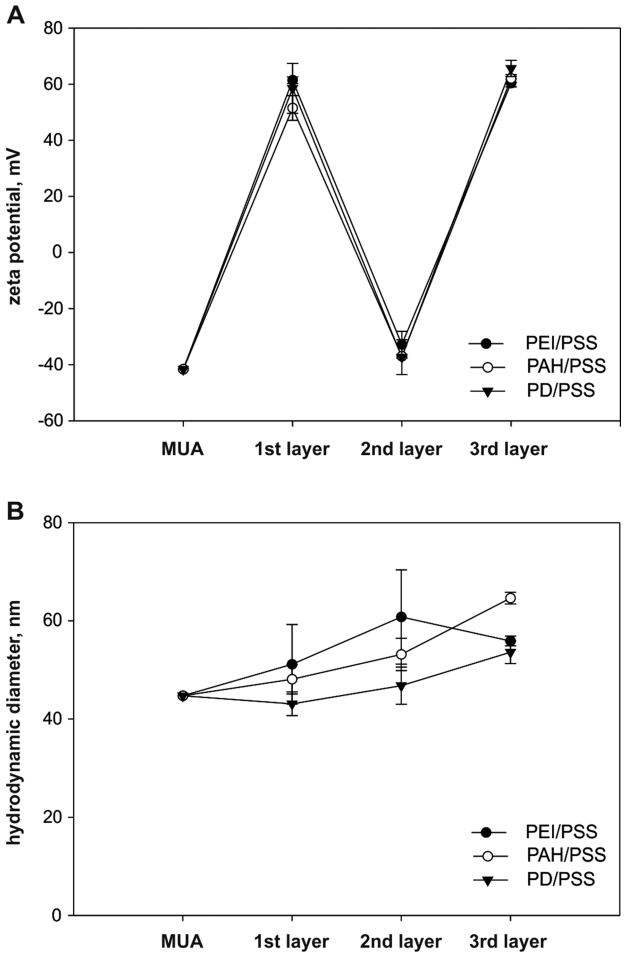

Figure 3. During oligolayer formation, the gold nanoparticles were characterized by their (A) zeta potential and (B) hydrodynamic diameter. The coating was performed from a single batch of synthesized and MUA-modified gold nanoparticles and was performed in at least triplicate.

coated gold nanoparticles and the decrease of Δ reflectivity in SPR were induced by an overshoot phenomenon.

Despite these differences during the assembly process, the nanoparticles were of similar size and zeta potential. Consequently, they were a favorable and well-defined tool to elucidate the influence of the surface appearance and texture on their interaction with biological systems.[49] When nanoparticles enter a biological environment, their surfaces will be decorated with serum proteins. Because it is known that the resulting protein corona is more decisive for nanoparticle fate in a biological context than the physicochemical properties themselves,[49] the protein corona after incubation with serum-containing cell culture medium was analyzed by SDS-PAGE as a first step. Although this technique only detects the most-abundant proteins, major differences concerning the total amount of proteins on a nanoparticles surface were resolved (Figure 4 A). The corresponding relative intensities of the SDS-PAGE protein lanes are illustrated in Figure 4 B. They demonstrate that the total protein adsorption served as a good validation that oligolayer-coated nanoparticles with comparable colloidal properties interact differently with serum proteins. Thus, the coating-series followed different trends from one coating level to the next. Within the PEI-series, the protein amount increased by a factor of ∼5 from the first to the second coating level, and increased an additional 12-fold for the last layer. The protein amount in the PAH-series first increased to the second coating level and then decreased upon the third layer resulting in only half the amount found with two layers. In the PD-series, the protein adsorption first slightly increased and then remained nearly constant for the next coating level. Surprisingly, although one could assume an identical surface coverage with negatively charged PSS at the second coating level, the intensities as well as the pattern of adsorbed proteins were different.

Because most serum proteins carry a net negative charge at physiological pH,[49] one would intuitively expect a higher amount of protein adsorption on the positively charged particles (i.e., particles with either one or three polymer layers). However, in the PAH-series for example, the bilayered negatively charged particles (PAH/PSS) showed the highest protein adsorption values. Consequently, differences among nanoparticles cannot be explained by electrostatics alone, and other factors seem to be important in shaping the protein corona. We searched for another critical particle property, and various possibilities were conceivable. The chemical identity (i.e., architecture, functional amino groups, and molecular weight) of polyelectrolytes definitively plays a role but cannot be solely responsible, because on the first coating level of each polycation, the total protein adsorption as well as the pattern of the protein bands were similar. The hydrophobicity of the surface is another aspect that is associated with protein adsorption.[50,51] Indeed, the hydrophobicity is highest for the trilayered PEI surface and decreases in the order PEI > PAH > PD (contact angles of approximately 81°, 74°, and 59°, respectively, see Supporting Information, Figure S5). However, the hydrophobicity similarly cannot be the sole reason because the PAH/PSS/PAH and PD/PSS/PD surfaces show, despite significant differences in their contact angles, a similar degree of protein adsorption. Thus, we speculated that the different layer deposition mechanisms and resulting surface topographies that were observed for their two-dimensional counterparts also had a tremendous impact on the deposition of serum proteins. Although comparing the results of a two-dimensional macroscopic substrate with a three-dimensional colloidal system is critical, a similar trend in the protein adsorption and root-mean-square surface roughness (Rq) was found (Table 3). For example, the trilayered sample of the PEI-series showed a very high surface roughness (Rq = 94.84 nm) and a topography with sharp surface features, and these nanoparticles also led to massive protein adsorption. Both the roughness and protein adsorption increased by a factor of ∼12 from the second to the third layer (Table 3). Here, one could even assume a synergistic effect of the electrostatic affinity of the polymer, its more hydrophobic surface, and the presence of more binding sites due to the higher surface roughness. In the the PD-series, both the bilayered and trilayered surfaces showed a comparable smooth topography in the AFM images and as well as comparable Rq values. At the same time, the protein adsorption was always in the same low range (Table 3). The low surface contact area, due to the absence of high surface features, most likely hindered adsorption of serum proteins. In samples belonging to the PAH-series, the surface roughness decreased from the second to the third layer. This decrease was also accompanied by a reduction in the amount of adsorbed proteins. Although there is no consensus on the precise effect of surface roughness on protein adsorption,[16] a number of reports have confirmed that a higher number of binding sites

DOI: 10.1021/am508435j
ACS Appl. Mater. Interfaces 2015, 7, 7891−7900

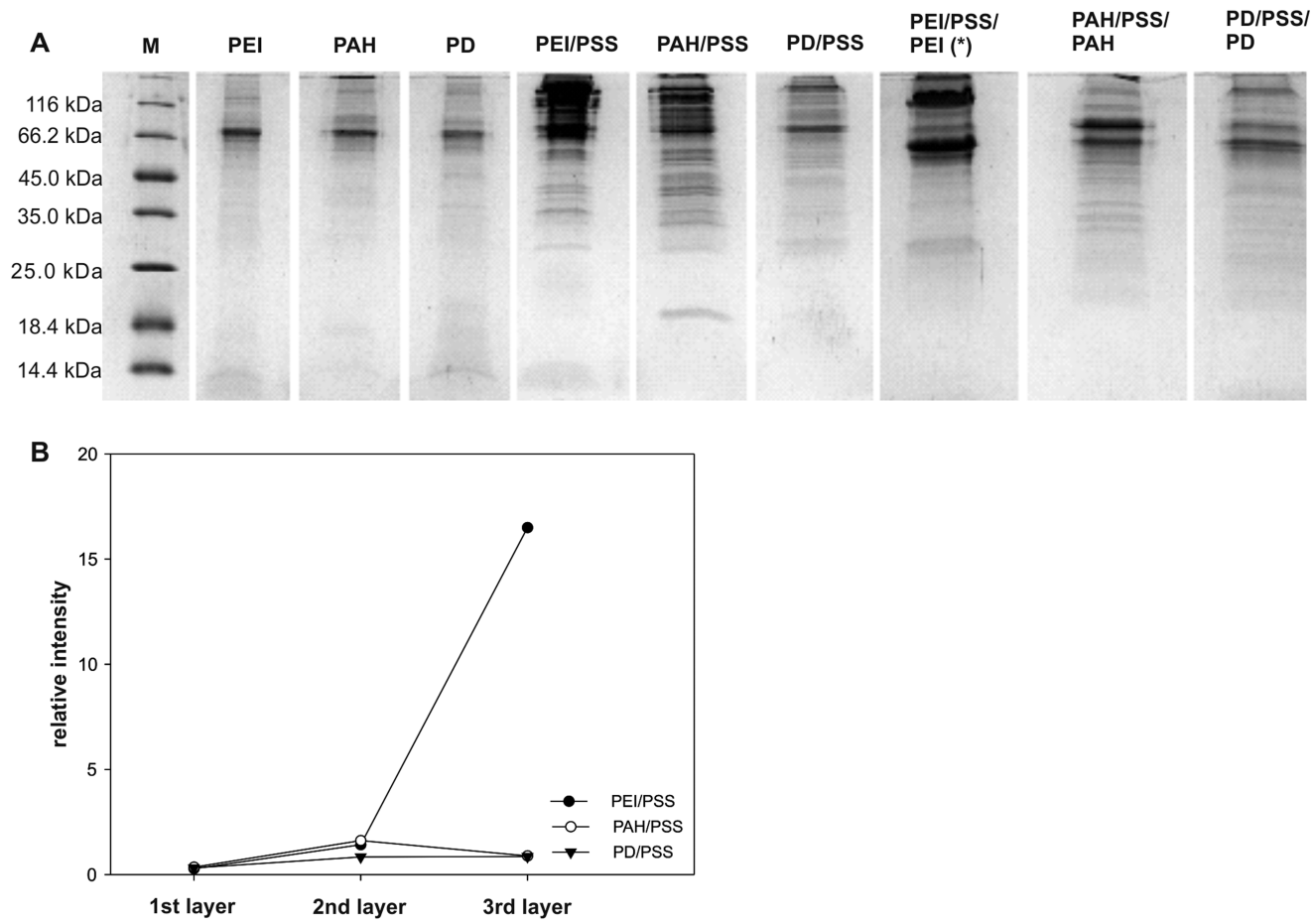

Figure 4. (A) Analysis of the protein corona of LbL-coated gold nanoparticles using SDS-PAGE. The protein molecular weight marker is indicated with M. The highest protein adsorption was found for the trilayered particles of the PEI-series (*). This sample had to be diluted by a factor of 12.5 compared to the other samples to get a clear protein separation pattern. (B) Comparison of the relative intensities determined from SDS-PAGE analysis. Standard deviations are absent because the values were extracted from one of two representative gel runs.

Table 3. Correlating Relative Protein Adsorption Data with Root-Mean-Square Surface Roughness (Rq) of the Bi- and Trilayered Samples

	PEI-series		PAH-series		PD-series	
	protein	Rq	protein	Rq	protein	Rq
second layer	1.42	8.08	1.62	17.31	0.84	21.58
third layer	16.50	94.84	0.89	14.76	0.86	29.12
relative change	11.62	11.74	0.55	0.85	1.02	1.35

available on rough surfaces can induce protein adsorption.[16,52,53]

In a drug delivery scenario, the adsorbed protein corona mediates cellular associations and subsequent uptake into cells.[49] Because protein adsorption was demonstrated to be a very sensitive marker for the surface properties of a colloid, the next step was to investigate if these differences were also reflected in cell associations. In general, the association of LbL-coated gold nanoparticles to HeLa cells, which are a commonly used model for nanoparticle cell interactions, increased at the applied concentrations without reaching a saturation level (Figure 5 A–C).

Interestingly, even at the stage of a single polymer layer, the cell association was different for each polyelectrolyte. Because they each had a similar amount of protein adsorption, this difference is likely attributable to polymer specific effects. The quaternary amines of PD seem to in general be less effective compared to the other amino groups as present in PEI and PAH. Therefore, it is also not surprising that polycations, particularly those containing lower order amino groups, are known to be effective transfection agents.[54] When comparing the cell association within one series from the second to the third coating step, further significant differences were observed, which also correlated well with the surface roughness of the materials. At stages of rougher surfaces within the PAH- and PEI-series, which were the PAH/PSS and PEI/PSS/PEI surfaces, respectively, cellular associations were reduced. On the other hand, they were enhanced for the smoother PAH/PSS/PAH and PEI/PSS surfaces of both series (Figure 5 A, B and Table 4). A similar trend concerning the cellular association and uptake was already reported for PAH/PSS-coated gold nanorods and was explained by the negatively charged cell membrane of HeLa cells repelling equally charged particles.[55] However, as the PAH/PSS and PEI/PSS surfaces carried a similar charge, electrostatics alone could again not be the only parameter responsible. On the other hand, the bi- and trilayered samples of the PD-series showed similar cell association values, which are also reflected by a similar extent of protein adsorption (Figure 5 C and Table 4). The corresponding toxicity data can be found in the Supporting Information, Figures S6 and S7).

DOI: 10.1021/am508435j
ACS Appl. Mater. Interfaces 2015, 7, 7891−7900

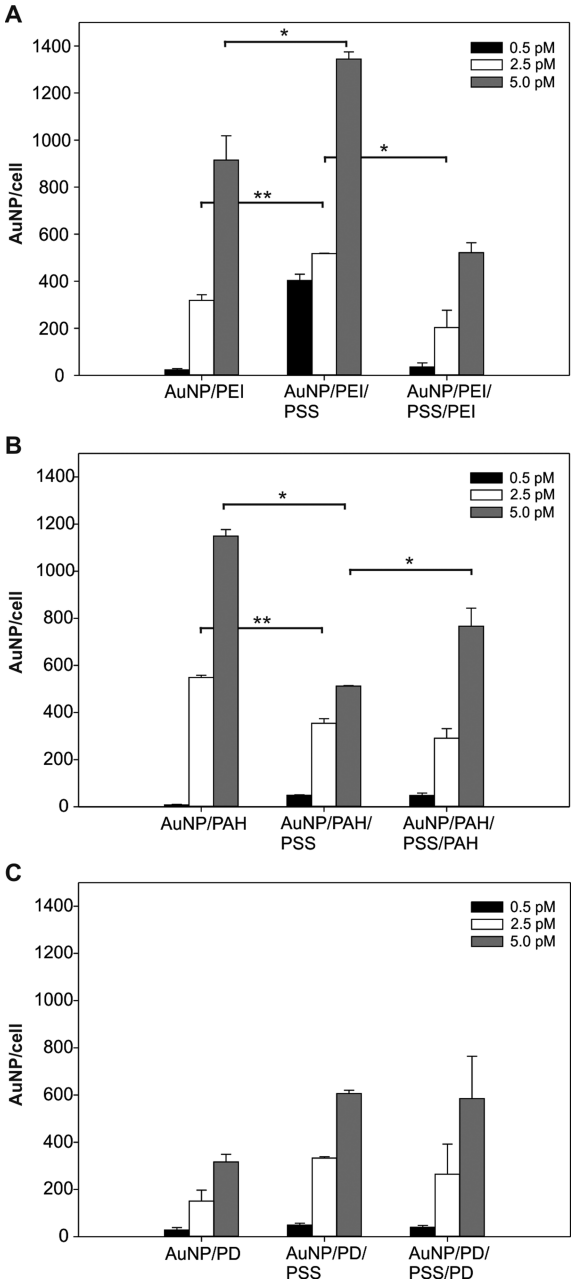

Figure 5. Cellular association of LbL-coated gold nanoparticles of the (A) PEI-, (B) PAH-, and (C) PD-series. In general, cellular associations increased with increasing particle concentration. In the PAH-series, the number of associated particles decreased from the first to the second layer, which is most likely due to the surface charge and enhanced protein adsorption. In contrast, in the PEI-series, the cell association increased from the first to the second layer and then decreased again with the third layer. This can again be explained by the correlation between protein adsorption and the surface topography. The cell association efficiency was similar for the bi- and trilayered particles of the PD-series. Statistically significant differences are indicated by * $p < 0.01$ and ** $p < 0.05$.

From these results, we conclude that the protein corona is extensively responsible for the cell association efficiency for our particles and that massive protein adsorption will have an inhibitory effect on the cellular associations. Although the total amount of proteins does not encode molecular details of nanoparticle surfaces that are important for cellular interactions, this correlation is possible for formulations with similar functional surface groups, as in our case.[49] Thus, we assumed that an optimal amount of adsorbed protein on the particle surface is necessary to enhance cellular associations. However, to evaluate the effects of the protein corona on the association to cells in a more detailed fashion, especially concerning its composition, further proteomic studies would be necessary.

Table 4. Correlating Relative Protein Adsorption with the Cellular Association of Bi- And Trilayered Samples

	PEI-series		PAH-series		PD-series	
	protein	cell assoc.	protein	cell assoc.	protein	cell assoc.
second layer	1.42	1450	1.62	500	0.84	600
third layer	16.50	500	0.89	750	0.86	600
relative change	11.62	0.34	0.55	1.50	1.02	1.00

CONCLUSION

We demonstrated that oligolayer deposition of various polycations in combination with a polyanion leads to significant differences in surface topography. When translating the characteristic surface features from a macroscopic substrate to colloidal gold nanoparticles of comparable physicochemical properties, tremendous differences in the interactions at the bionano interface were observed. We conclude that the surface topography of the LbL-coated nanoparticles is decisive for the adsorption of serum proteins and later the association with cells. Thus, a pronounced surface roughness leads to massive protein adsorption due to a larger surface contact area and consequently to reduced cellular associations. On the basis of our findings, we strongly recommend that, in the case of LbL-coated nanoparticles for drug delivery applications, the oligolayer deposition mechanisms and the resulting surface topographies should be considered as important nanoparticle characteristics. In this way, another parameter aside from particle size, charge, and hydrophobicity can help to estimate the efficacy of oligolayer-coated nanoparticles for drug delivery.

ASSOCIATED CONTENT

Supporting Information

Fitting parameters for SPR measurements, high resolution AFM images, water contact angle measurements, and toxicity data. This material is available free of charge via the Internet at http://pubs.acs.org.

AUTHOR INFORMATION

Corresponding Author

*E-mail: Miriam.Breunig@chemie.uni-regensburg.de.

Present Address

§R.R.: Institute of Inorganic and Analytical Chemistry, Johannes Gutenberg University Mainz, Duesbergweg 10−14, 55128 Mainz, Germany

Notes

The authors declare no competing financial interest.

ACKNOWLEDGMENTS

The authors thank Edith Schindler for her technical assistance in the protein adsorption experiments, Kelsey Erin Knewtson for proofreading of the manuscript, and Johannes Thoma for his work on the photometric cell association assay. This project was financially supported by the Deutsche Forschungsgemeinschaft (DFG, Grant BR 3566/2-1).

DOI: 10.1021/am508435j
ACS Appl. Mater. Interfaces 2015, 7, 7891−7900

REFERENCES

(1) Boudou, T.; Crouzier, T.; Ren, K.; Blin, G.; Picart, C. Multiple Functionalities of Polyelectrolyte Multilayer Films: New Biomedical Applications. *Adv. Mater.* **2010**, *22*, 441−467.

(2) Yan, Y.; Björnmalm, M.; Caruso, F. Assembly of Layer-by-Layer Particles and Their Interactions with Biological Systems. *Chem. Mater.* **2014**, 452−460.

(3) Hammond, P. T. Polyelectrolyte Multilayered Nanoparticles: Using Nanolayers for Controlled and Targeted Systemic Release. *Nanomedicine* **2012**, *7*, 619−622.

(4) *Multilayer Thin Films*; Decher, G., Schlenoff, J. B., Eds.; Wiley-VCH: Weinheim, Germany, 2003.

(5) *Multilayer Thin Films*; Decher, G., Schlenoff, J. B., Eds.; Wiley-VCH: Weinheim, Germany, 2012.

(6) Schneider, G.; Decher, G. Functional Core/Shell Nanoparticles via Layer-by-Layer Assembly. Investigation of the Experimental Parameters for Controlling Particle Aggregation and for Enhancing Dispersion Stability. *Langmuir* **2008**, *24*, 1778−1789.

(7) Schneider, G.; Decher, G. From Functional Core/Shell Nanoparticles Prepared via Layer-by-Layer Deposition to Empty Nanospheres. *Nano Lett.* **2004**, *4*, 1833−1839.

(8) Elbakry, A.; Zaky, A.; Liebl, R.; Rachel, R.; Goepferich, A.; Breunig, M. Layer-by-Layer Assembled Gold Nanoparticles for siRNA Delivery. *Nano Lett.* **2009**, *9*, 2059−2064.

(9) Deng, Z. J.; Morton, S. W.; Ben-Akiva, E.; Dreaden, E. C.; Shopsowitz, K. E.; Hammond, P. T. Layer-by-Layer Nanoparticles for Systemic Codelivery of an Anticancer Drug and siRNA for Potential Triple-Negative Breast Cancer Treatment. *ACS Nano* **2013**, *7*, 9571−9584.

(10) Dreaden, E. C.; Morton, S. W.; Shopsowitz, K. E.; Choi, J.-H.; Deng, Z. J.; Cho, N.-J.; Hammond, P. T. Bimodal Tumor-Targeting From Microenvironment Responsive Hyaluronan Layer-by-Layer (LbL) Nanoparticles. *ACS Nano* **2014**, *8*, 8374−8382.

(11) Han, L.; Zhao, J.; Zhang, X.; Cao, W.; Hu, X.; Zou, G.; Duan, X.; Liang, X.-J. Enhanced siRNA Delivery and Silencing Gold−Chitosan Nanosystem with Surface Charge-Reversal Polymer Assembly and Good Biocompatibility. *ACS Nano* **2012**, *6*, 7340−7351.

(12) Tan, Y. F.; Mundargi, R. C.; Chen, M. H. A.; Lessig, J.; Neu, B.; Venkatraman, S.; Wong, T. T. Layer-by-Layer Nanoparticles as an Efficient siRNA Delivery Vehicle for SPARC Silencing. *Small* **2014**, *10*, 1790−1798.

(13) Elbakry, A.; Wurster, E.-C.; Zaky, A.; Liebl, R.; Schindler, E.; Bauer-Kreisel, P.; Blunk, T.; Goepferich, A.; Breunig, M. Layer-by-Layer Coated Gold Nanoparticles: Size-Dependent Delivery of DNA Into Cells. *Small* **2012**, *8*, 3847−3856.

(14) Morton, S. W.; Herlihy, K. P.; Shopsowitz, K. E.; Deng, Z. J.; Chu, K. S.; Bowerman, C. J.; DeSimone, J. M.; Hammond, P. T. Scalable Manufacture of Built-to-Order Nanomedicine: Spray-Assisted Layer-by-Layer Functionalization of PRINT Nanoparticles. *Adv. Mater.* **2013**, *25*, 4707−4713.

(15) Chithrani, B. D.; Ghazani, A. A.; Chan, W. C. W. Determining the Size and Shape Dependence of Gold Nanoparticle Uptake Into Mammalian Cells. *Nano Lett.* **2006**, *6*, 662−668.

(16) Scopelliti, P. E.; Borgonovo, A.; Indrieri, M.; Giorgetti, L.; Bongiorno, G.; Carbone, R.; Podestà, A.; Milani, P. The Effect of Surface Nanometre-Scale Morphology on Protein Adsorption. *PLoS One* **2010**, *5*, e11862.

(17) Wong, S. Y.; Han, L.; Timachova, K.; Veselinovic, J.; Hyder, M. N.; Ortiz, C.; Klibanov, A. M.; Hammond, P. T. Drastically Lowered Protein Adsorption on Microbicidal Hydrophobic/Hydrophilic Polyelectrolyte Multilayers. *Biomacromolecules* **2012**, *13*, 719−726.

(18) Wastl, D. S.; Speck, F.; Wutscher, E.; Ostler, M.; Seyller, T.; Giessibl, F. J. Observation of 4 nm Pitch Stripe Domains Formed by Exposing Graphene to Ambient Air. *ACS Nano* **2013**, *7*, 10032−10037.

(19) Wastl, D. S.; Weymouth, A. J.; Giessibl, F. J. Atomically Resolved Graphitic Surfaces in Air by Atomic Force Microscopy. *ACS Nano* **2014**, *8*, 5233−5239.

(20) Wastl, D. S.; Weymouth, A. J.; Giessibl, F. J. Optimizing Atomic Resolution of Force Microscopy in Ambient Conditions. *Phys. Rev. B* **2013**, *87*, 245415.

(21) Wastl, D. S.; Judmann, M.; Weymouth, A. J.; Giessibl, F. J. Giessibl Atomic Resolution of Calcium and Oxygen Sublattices of Calcite in Ambient Conditions by Atomic Force Microscopy Using qPlus Sensors with Sapphire Tips. 10.1021/acsnano.5b01549.

(22) Schneiderbauer, M.; Wastl, D.; Giessibl, F. J. qPlus Magnetic Force Microscopy in Frequency-Modulation Mode with Millihertz Resolution. *Beilstein J. Nanotechnol.* **2012**, *3*, 174−178.

(23) Giessibl, F. J. Atomic Resolution on Si(111)-(7 × 7) by Noncontact Atomic Force Microscopy with a Force Sensor Based on a Quartz Tuning Fork. *Appl. Phys. Lett.* **2000**, *76*, 1470.

(24) Horcas, I.; Fernández, R.; Gómez-Rodríguez, J. M.; Colchero, J.; Gómez-Herrero, J.; Baro, A. M. WSXM: a Software for Scanning Probe Microscopy and a Tool for Nanotechnology. *Rev. Sci. Instrum.* **2007**, *78*, 013705.

(25) Wurster, E.-C.; Elbakry, A.; Goepferich, A.; Breunig, M. Layer-by-Layer Assembled Gold Nanoparticles for the Delivery of Nucleic Acids. In *Nanotechnology for Nucleic Acid Delivery: Methods and Protocols*; Ogris, M., Oupicky, D., Eds.; Methods in Molecular Biology; Humana Press: Totowa, NJ, 2012; Chapter 12, pp 171−182.

(26) Balasubramanian, S. K.; Yang, L.; Yung, L.-Y. L.; Ong, C.-N.; Ong, W.-Y.; Yu, L. E. Characterization, Purification, and Stability of Gold Nanoparticles. *Biomaterials* **2010**, *31*, 9023−9030.

(27) Liu, X.; Atwater, M.; Wang, J.; Huo, Q. Extinction Coefficient of Gold Nanoparticles with Different Sizes and Different Capping Ligands. *Colloids Surf. B Biointerfaces* **2007**, *58*, 3−7.

(28) Lundquist, M.; Stigler, J.; Elia, G.; Lynch, I.; Cedervall, T.; Dawson, K. A. Nanoparticle Size and Surface Properties Determine the Protein Corona with Possible Implications for Biological Impacts. *Proc. Natl. Acad. Sci. U.S.A.* **2008**, *105*, 14265−14270.

(29) Cho, E. C.; Liu, Y.; Xia, Y. A Simple Spectroscopic Method for Differentiating Cellular Uptakes of Gold Nanospheres and Nanorods From Their Mixtures. *Angew. Chem., Int. Ed.* **2010**, *49*, 1976−1980.

(30) Cho, E. C.; Zhang, Q.; Xia, Y. The Effect of Sedimentation and Diffusion Oncellular Uptake of Gold Nanoparticles. *Nat. Nanotechnol.* **2011**, *6*, 385−391.

(31) Neu, M.; Fischer, D.; Kissel, T. Recent Advances in Rational Gene Transfer Vector Design Based on Poly(Ethylene Imine) and Its Derivatives. *J. Gene Med.* **2005**, *7*, 992−1009.

(32) Silva, C. P.; Carapuça, H. M. Glassy Carbon Electrodes Coated with Poly(Allylamine Hydrochloride), PAH: Characterization Studies and Application to Ion-Exchange Voltammetry of Trace Lead(II) at Combined PAH/Mercury Film Electrodes. *Electrochim. Acta* **2006**, *52*, 1182−1190.

(33) Monterroso, S.; Carapuca, K.; Duarte, A. Mixed Polyelectrolyte Coatings on Glassy Carbon Electrodes: Ion-Exchange, Permselectivity Properties and Analytical Application of Poly-L-Lysine−Poly(Sodium 4-Styrenesulfonate)-Coated Mercury Film Electrodes for the Detection of Trace Metals. *Talanta* **2006**, *68*, 1655−1662.

(34) lungwitz, U.; Breunig, M.; Blunk, T.; Göpferich, A. Polyethylenimine-Based Non-Viral Gene Delivery Systems. *Eur. J. Pharm. Biopharm.* **2005**, *60*, 247−266.

(35) Klitzing; von, R. Internal Structure of Polyelectrolyte Multilayer Assemblies. *Phys. Chem. Chem. Phys.* **2006**, *8*, 5012.

(36) Plunkett, M. A.; Wang, Z.; Rutland, M. W.; Johannsmann, D. Adsorption of pNIPAM Layers on Hydrophobic Gold Surfaces, Measured in Situ by QCM and SPR. *Langmuir* **2003**, *19*, 6837−6844.

(37) Yoo, D.; Shiratori, S. S.; Rubner, M. F. Controlling Bilayer Composition and Surface Wettability of Sequentially Adsorbed Multilayers of Weak Polyelectrolytes. *Macromolecules* **1998**, *31*, 4309−4318.

(38) Shiratori, S. S.; Rubner, M. F. pH-Dependent Thickness Behavior of Sequentially Adsorbed Layers of Weak Polyelectrolytes. *Macromolecules* **2000**, *33*, 4213−4219.

(39) Gong, H.; Garcia-Turiel, J.; Vasilev, K.; Vinogradova, O. I. Interaction and Adhesion Properties of Polyelectrolyte Multilayers. *Langmuir* **2005**, *21*, 7545−7550.

DOI: 10.1021/am508435j
ACS Appl. Mater. Interfaces 2015, 7, 7891−7900

(40) Caruso, F.; Niikura, K.; Furlong, D. N.; Okahata, Y. 1. Ultrathin Multilayer Polyelectrolyte Films on Gold: Construction and Thickness Determination. *Langmuir* **1997**, *13*, 3422−3426.
(41) Kovacevic, D.; van der Burgh, S.; de Keizer, A.; Cohen Stuart, M. A. Kinetics of Formation and Dissolution of Weak Polyelectrolyte Multilayers: Role of Salt and Free Polyions. *Langmuir* **2002**, *18*, 5607−5612.
(42) Filippov, L. K.; Filippova, N. L. Overshoots of Adsorption Kinetics. *J. Colloid Interface Sci.* **1996**, *178*, 571−580.
(43) Buron, C. C.; Filiâtre, C. Overshoots of Adsorption Kinetics During Layer-by-Layer Polyelectrolyte Film Growth: Role of Counterions. *J. Colloid Interface Sci.* **2014**, *413*, 147−153.
(44) Buron, C. C.; Filiâtre, C.; Membrey, F.; Bainier, C.; Charraut, D.; Foissy, A. Early Steps in Layer-by-Layer Construction of Polyelectrolyte Films: the Transition From Surface/Polymer to Polymer/Polymer Determining Interactions. *J. Colloid Interface Sci.* **2007**, *314*, 358−366.
(45) Wiśniewska, M.; Urban, T.; Grządka, E.; Zarko, V. I.; Gun'ko, V. M. Comparison of Adsorption Affinity of Polyacrylic Acid for Surfaces of Mixed Silica−Alumina. *Colloid Polym. Sci.* **2014**, *292*, 699−705.
(46) McAloney, R. A.; Sinyor, M.; Dudnik, V.; Goh, M. C. Atomic Force Microscopy Studies of Salt Effects on Polyelectrolyte Multilayer Film Morphology. *Langmuir* **2001**, *17*, 6655−6663.
(47) Netz, R. R.; Joanny, J.-F. Adsorption of Semiflexible Polyelectrolytes on Charged Planar Surfaces: Charge Compensation, Charge Reversal, and Multilayer Formation. *Macromolecules* **1999**, *32*, 9013−9025.
(48) Nestler, P.; Paßvogel, M.; Helm, C. A. Influence of Polymer Molecular Weight on the Parabolic and Linear Growth Regime of PDADMAC/PSS Multilayers. *Macromolecules* **2013**, *46*, 5622−5629.
(49) Walkey, C. D.; Olsen, J. B.; Song, F.; Liu, R.; Guo, H.; Olsen, D. W. H.; Cohen, Y.; Emili, A.; Chan, W. C. W. Protein Corona Fingerprinting Predicts the Cellular Interaction of Gold and Silver Nanoparticles. *ACS Nano* **2014**, *8*, 2439−2455.
(50) Walkey, C. D.; Chan, W. C. W. Understanding and Controlling the Interaction of Nanomaterials with Proteins in a Physiological Environment. *Chem. Soc. Rev.* **2012**, *41*, 2780.
(51) Gunawan, C.; Lim, M.; Marquis, C. P.; Amal, R. Nanoparticle−Protein Corona Complexes Govern the Biological Fates and Functions of Nanoparticles. *J. Mater. Chem. B* **2014**, *2*, 2060.
(52) Rechendorff, K.; Hovgaard, M. B.; Foss, M.; Zhdanov, V. P.; Besenbacher, F. Enhancement of Protein Adsorption Induced by Surface Roughness. *Langmuir* **2006**, *22*, 10885−10888.
(53) Ercan, B.; Khang, D.; Carpenter, J.; Webster, T. Using Mathematical Models to Understand the Effect of Nanoscale Roughness on Protein Adsorption for Improving Medical Devices. *Int. J. Nanomed.* **2013**, *8*, 75−81.
(54) Nguyen, J.; Szoka, F. C. Nucleic Acid Delivery: the Missing Pieces of the Puzzle? *Acc. Chem. Res.* **2012**, *45*, 1153−1162.
(55) Szabo, I.; Brutsche, S.; Tombola, F.; Moschioni, M.; Satin, B.; Telford, J. L.; Rappuoli, R.; Montecucco, C.; Papini, E. Formation of Anion-Selective Channels in the Cell Plasma Membrane by the Toxin VacA of *Helicobacter pylori* Is Required for Its Biological Activity. *EMBO J.* **1999**, *18*, 5517−5527.

DOI: 10.1021/am508435j
ACS Appl. Mater. Interfaces 2015, 7, 7891−7900